Communications in Nonlinear Science and Numerical Simulation 108 (2022) 106246

Contents lists available at ScienceDirect

Communications in Nonlinear Science and Numerical Simulation

journal homepage: www.elsevier.com/locate/cnsns

Research paper

The effect of coherent coupling nonlinearity on modulation instability and rogue wave excitation

Heping Jia [a,b], Rongcao Yang [a,b,*], Qi Guo [c], J.M. Christian [d]

[a] School of Physics and Electronic Engineering, Shanxi University, Taiyuan 030006, China
[b] Collaborative Innovation Center of Extreme Optics, Shanxi University, Taiyuan, 03006, China
[c] Guangdong Provincial Key Laboratory of Nanophotonic Functional Materials and Devices, South China Normal University, Guangzhou, 510631, China
[d] Joule Physics Laboratory, School of Science, Engineering and Environment, University of Salford, Greater Manchester, M5 4WT, UK

ARTICLE INFO

Article history:
Received 29 September 2021
Received in revised form 23 December 2021
Accepted 30 December 2021
Available online 10 January 2022

Keywords:
Modulation instability
Rogue wave
Coherent coupling nonlinearity
Nonlinear Schrödinger equations

ABSTRACT

We study modulation instability (MI) in both anomalous and normal dispersion regimes of a coherently coupled system. It is found that there exist three types of MI spectra with distinct characteristics termed baseband, passband, and zero-baseband based on the instability analysis of the in-phase and out-of-phase CW solutions. The coherent coupling nonlinearity is the source of the passband and zero-baseband variants. Guided by analytical predictions, we investigate numerically the excitation of rogue waves on weakly perturbed in-phase and out-of-phase continuous wave solutions in the parameter space where different kinds of MI exist. Simulations provide supporting evidence that rogue waves can only emerge in regimes where baseband or zero-baseband MI occurs. Moreover, the peak intensity of rogue waves in the case of baseband MI is greater than in the zero-baseband case. Finally, a combination of analysis and numerics uncovers the parameter conditions necessary for the generation of rogue waves.

1. Introduction

Rogue waves (RWs) – initially observed as giant waves appearing suddenly on the ocean surface – have become important when describing nonlinear phenomena across many physical contexts [1–7]. Although some uncertainty still remains on the exact origins of RWs, there is general agreement that modulation instability (MI) and the collision of breathers are important building blocks [8–12]. Recently, researchers found that MI is a necessary but not sufficient condition for RW generation [13–15]. In other words, some kinds of MI are not responsible for the excitation of RWs. Within the framework of the Manakov and Fokas–Lenells equations, Baronio et al. [13,14] discovered that baseband MI (defined as the spectral region of MI containing the zero-frequency perturbation as a limiting case) coincides with RW generation, while passband MI (the spectral region of MI not including the zero-frequency perturbation) leads only to a train of nonlinear oscillations. Also importantly, Zhao et al. [15] found that RWs may emerge from MI with a resonance perturbation by investigating the connections between instability and several nonlinear waves governed by nonlinear Schrödinger (NLS) equations. Chen et al. [16,17] investigated the emergence of RWs on top of periodic standing waves and their relation to the MI properties of those standing waves. Therefore, a detailed study of MI and its link to RWs in different nonlinear systems is instructive for uncovering the true origin of RWs.

* Corresponding author at: School of Physics and Electronic Engineering, Shanxi University, Taiyuan 030006, China.
E-mail address: sxdxyrc@sxu.edu.cn (R. Yang).

https://doi.org/10.1016/j.cnsns.2021.106246
1007-5704/

MI describes the exponential growth of small perturbations on a continuous wave (CW) background. It is related to many important nonlinear processes in addition to RW formation, such as supercontinuum generation [18] and soliton generation [19]. Although linear analysis has limitations that have been corrected using a weakly nonlinear theory of wave propagation, it still plays a significant role when assessing MI characteristics [20,21]. Based on linear stability analysis, it has been found that the MI of freely-propagating waves only occurs in the focusing regime for a nonlinear system governed by the standard NLS equation [20]. However, in multi-component generalizations, the focusing regime is not a necessary condition for MI. For example, MI can exist in the defocusing regime due to the cross-phase modulation between two different waves [22,23]; subsequent experiments with two polarization modes [24,25] verified that theoretical prediction. Indeed, MI in multi-component systems is a more complicated problem than in typical single-component systems, and so they potentially yield new and rich RW patterns [26–28]. For example, Chan et al. [26] discovered additional MI regimes and novel RW structures linked to group-velocity mismatch in coupled multi-wave systems. The novel wave-based phenomena found in coherently coupled systems give rise to additional complexity due to the existence of additional mechanisms for energy transfer between the two constituent waves [29,30].

An obvious question to pose is, what happens to perturbed CW solutions in coherently coupled systems with different parameters? Furthermore, in which parameter spaces can RWs be excited? And what is the difference between the properties of RWs in the various parameter spaces? To answer these questions, in Section 2 we investigate MI in a coherently coupled nonlinear system by using linear stability analysis, and discuss the influence of coherent coupling on MI spectra. Based on that analysis, in Section 3 we study numerically the emergence of RWs in parameter spaces where different kinds of MI are present. We also obtain the parameter conditions for RW generation. Conclusions are drawn in Section 4.

2. Modulation instability in the coherently coupled nonlinear Schrödinger system

A coherently coupled nonlinear system can be described by the following system of two dimensionless NLS-type equations [29],

$$i\frac{\partial u}{\partial z}+\beta\frac{\partial^2 u}{\partial t^2}+\gamma_1|u|^2u+\gamma_2|v|^2u+\gamma_3v^2u^*=0, \tag{1a}$$

$$i\frac{\partial v}{\partial z}+\beta\frac{\partial^2 v}{\partial t^2}+\gamma_1|v|^2v+\gamma_2|u|^2v+\gamma_3u^2v^*=0. \tag{1b}$$

Here, u and v are the wave envelopes, γ_1 represents the nonlinearity coefficient, while γ_2 and γ_3 denote incoherent and coherent coupling coefficients, respectively. In nonlinear fiber models, z and t are the propagation distance and time respectively; γ_1 and γ_2 are the self- and cross-phase modulation coefficients, respectively, while γ_3 is the four-wave mixing coefficient (which can be neglected in the case of large birefringence) [30,31]. In the context of Bose–Einstein condensates, z and t are, respectively, the time and the space coordinates; γ_1 and γ_2 are the intra- and inter-component strengths, while γ_3 describes the pair-transition effect caused by the interaction between atoms [32].

System (1) has the CW solution

$$u_{01}(z,t)=A_0\exp\left[i(\alpha z+\omega t)\right], \tag{2a}$$

$$v_{01}(z,t)=\pm A_0\exp\left[i(\alpha z+\omega t)\right]. \tag{2b}$$

Here, A_0, ω and $\alpha=(\gamma_1+\gamma_2+\gamma_3)A_0^2-\beta\omega^2$ are the amplitude, frequency, and wave number, respectively. These waves are in-phase or out-of-phase when the "+" or "−" sign, respectively, is adopted in Eq. (2b).

For $\gamma_3=\gamma_1-\gamma_2$, system (1) possesses the more general CW solution

$$u_{02}(z,t)=A_1\exp\left[i(\alpha z+\omega t)\right], \tag{3a}$$

$$v_{02}(z,t)=A_2\exp\left[i(\alpha z+\omega t)\right], \tag{3b}$$

where $\alpha=\gamma_1(A_1^2+A_2^2)-\beta\omega^2$. Finally, when $\gamma_1=\gamma_2=\gamma$ and $\gamma_3=0$, system (1) reduces to the Manakov equation, for which the well-known CW solution is [13,33]

$$u_{03}(z,t)=A_1\exp\left[i(\alpha_1 z+\omega_1 t)\right], \tag{4a}$$

$$v_{03}(z,t)=A_2\exp\left[i(\alpha_2 z+\omega_2 t)\right], \tag{4b}$$

where $\alpha_j=\gamma(A_1^2+A_2^2)-\beta\omega_j^2, j=1,2$.

The effect of birefringence on the MI of CW solution (3) is studied in Ref. [27], and RWs with ultra-high amplitudes are presented in Ref. [29]. The link between the type of MI and RWs in the Manakov system is revealed in Ref. [13] by comparing the existence condition of the RW solution and the parameter spaces where different MI regimes occur. Here, we are interested in quantifying how novel effects arising from the interactions between parameters γ_1, γ_2 and γ_3 impact

their MI spectra and potential for RW generation. Therefore, we consider CW solution (2) and begin by perturbing it according to

$$u(z,t) = u_{01}(z,t)\,[1 + q_1(z,t)]\,, \tag{5a}$$

$$v(z,t) = v_{01}(z,t)\,[1 + q_2(z,t)]\,. \tag{5b}$$

The functions q_1 and q_2 represent weak perturbations (i.e., having magnitudes much less than unity) in the two components. Substituting Eq. (5) into Eq. (1) and ignoring high-order terms of perturbation, one can obtain the following linearized equations

$$iq_{1z} + 2i\beta\omega q_{1t} + \beta q_{1tt} + (\gamma_1+\gamma_3)A_0^2 q_1^* + (\gamma_1-\gamma_3)A_0^2 q_1 + \gamma_2 A_0^2 q_2^* + (\gamma_2+2\gamma_3)A_0^2 q_2 = 0, \tag{6a}$$

$$iq_{2z} + 2i\beta\omega q_{2t} + \beta q_{2tt} + (\gamma_1+\gamma_3)A_0^2 q_2^* + (\gamma_1-\gamma_3)A_0^2 q_2 + \gamma_2 A_0^2 q_1^* + (\gamma_2+2\gamma_3)A_0^2 q_1 = 0. \tag{6b}$$

Assuming q_1 and q_2 have the form [20,22,34,35]

$$q_1(z,t) = q_{11}\exp\left[i(Kz-\Omega t)\right] + q_{12}\exp\left[-i(Kz-\Omega t)\right], \tag{7a}$$

$$q_2(z,t) = q_{21}\exp\left[i(Kz-\Omega t)\right] + q_{22}\exp\left[-i(Kz-\Omega t)\right], \tag{7b}$$

where K and Ω are the wave number and frequency, respectively, of those perturbations, we substitute ansatz (7) into Eq. (6), and then obtain a set of four linear coupled equations which may be written as follows

$$\begin{bmatrix} \chi + 2\beta\omega\Omega - K & A_0^2(\gamma_1+\gamma_3) & A_0^2(\gamma_2+2\gamma_3) & A_0^2\gamma_2 \\ A_0^2(\gamma_1+\gamma_3) & \chi - 2\beta\omega\Omega + K & A_0^2\gamma_2 & A_0^2(\gamma_2+2\gamma_3) \\ A_0^2(\gamma_2+2\gamma_3) & A_0^2\gamma_2 & \chi + 2\beta\omega\Omega - K & A_0^2(\gamma_1+\gamma_3) \\ A_0^2\gamma_2 & A_0^2(\gamma_2+2\gamma_3) & A_0^2(\gamma_1+\gamma_3) & \chi - 2\beta\omega\Omega + K \end{bmatrix} \begin{bmatrix} q_{11} \\ q_{12} \\ q_{21} \\ q_{22} \end{bmatrix} = 0, \tag{8}$$

where $\chi = A_0^2\gamma_1 - \beta\Omega^2 - A_0^2\gamma_3$.

In order to admit nontrivial solutions, the determinant of the 4×4 matrix in Eq. (8) is required to vanish, which results in the following dispersion relation

$$K^4 + B_3K^3 + B_2K^2 + B_1K + B_0 = 0, \tag{9}$$

where

$$\begin{aligned} B_0 = {} & \beta\Omega^2\left\{16\gamma_3A_0^6\left[\gamma_1^2 - (\gamma_2+\gamma_3)^2\right] - 4\beta^2\Omega^2A_0^2(\gamma_1-\gamma_3)(\Omega^2-4\omega^2) + \beta^3(\Omega^3-4\omega^2\Omega)^2\right. \\ & \left. + 4\beta A_0^4\left[\gamma_1^2\Omega^2 - \gamma_2^2\Omega^2 + \gamma_1\gamma_3(8\omega^2-4\Omega^2) - 2\gamma_2\gamma_3(4\omega^2+\Omega^2) - \gamma_3^2(8\omega^2+\Omega^2)\right]\right\}, \end{aligned} \tag{10a}$$

$$B_1 = 8\beta\omega\Omega\left[4\gamma_3A_0^4(\gamma_1-\gamma_2-\gamma_3) + 2\beta\Omega^2A_0^2(\gamma_1-\gamma_3) - \beta^2\Omega^2(\Omega^2-4\omega^2)\right], \tag{10b}$$

$$B_2 = 8\gamma_3A_0^4(\gamma_1-\gamma_2-\gamma_3) + 4\beta\Omega^2A_0^2(\gamma_1-\gamma_3) - 2\beta^2\Omega^2(\Omega^2-12\omega^2), \tag{10c}$$

$$B_3 = -8\beta\omega\Omega. \tag{10d}$$

Dispersion relation (9) possesses two pairs of roots,

$$K_{1,2} = 2\beta\omega\Omega \pm |\beta|\sqrt{\Delta_1}, \tag{11a}$$

$$K_{3,4} = 2\beta\omega\Omega \pm |\beta|\sqrt{\Delta_2}, \tag{11b}$$

where the discriminants are

$$\Delta_1 = \Omega^2\left(\Omega^2 - \frac{2A_0^2(\gamma_1+\gamma_2+\gamma_3)}{\beta}\right), \tag{12a}$$

$$\Delta_2 = \left(\Omega^2 + \frac{4A_0^2\gamma_3}{\beta}\right)\left[\Omega^2 - \frac{2A_0^2(\gamma_1-\gamma_2-\gamma_3)}{\beta}\right]. \tag{12b}$$

Since MI arises from a non-vanishing imaginary part of K, the signs of the discriminants in Eqs. (12a) and (12b) are associated with the existence of any instability. CW solution (2) is thus robust against small perturbations when Δ_1 and

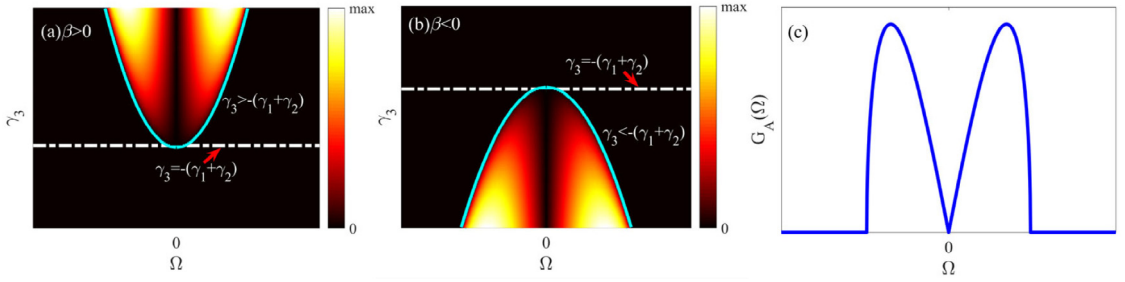

Fig. 1. Schematic plots of MI-A gain as functions of frequency Ω and coherent coupling nonlinearity γ_3 in the (a) anomalous and (b) normal dispersion regimes. (c) The cross-sectional views of (a) for $\gamma_3 > -(\gamma_1+\gamma_2)$ and (b) for $\gamma_3 < -(\gamma_1+\gamma_2)$. The cyan solid lines in (a) and (b) represent $\Omega^2 = 2A_0^2(\gamma_1+\gamma_2+\gamma_3)/\beta$. The adopted parameters are $\gamma_1 = 1$, $\gamma_2 = -2$, (a) $\beta = 1$, (b) $\beta = -1$.

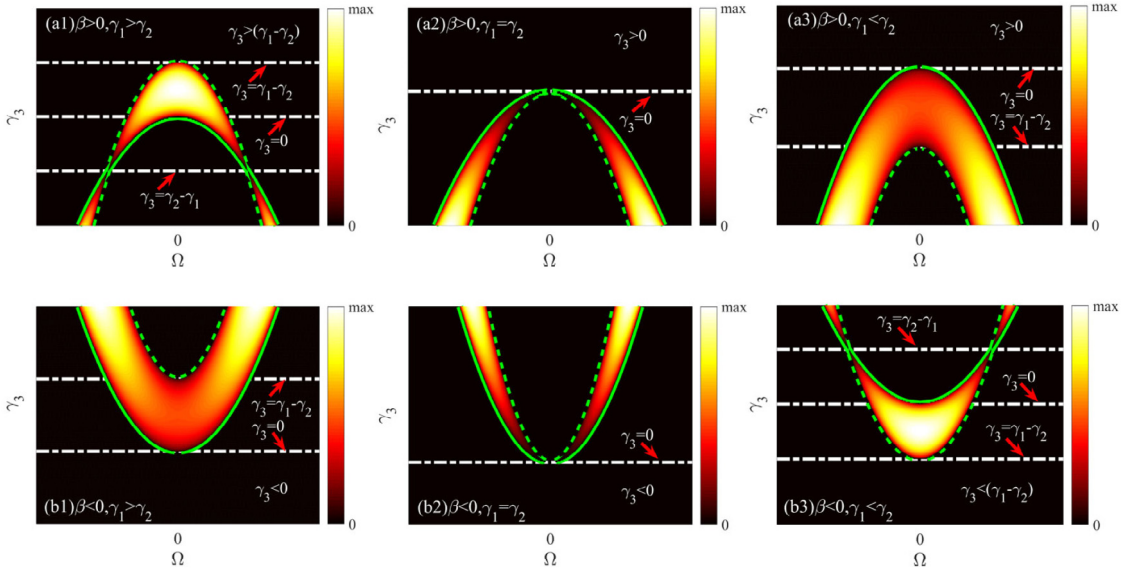

Fig. 2. Schematic plots of MI-B gain as functions of frequency Ω and coherent coupling nonlinearity γ_3 in the (a) anomalous and (b) normal dispersion regimes for different relations between γ_1 and γ_2. The green solid line and green dotted line denote $\Omega^2 = -4A_0^2\gamma_3/\beta$ and $\Omega^2 = 2A_0^2(\gamma_1-\gamma_2-\gamma_3)/\beta$, respectively. The adopted parameters are $\gamma_1 = 1$, (a1) $\beta = 1$, $\gamma_2 = -2$, (a2) $\beta = 1$, $\gamma_2 = 1$, (a3) $\beta = 1$, $\gamma_2 = 2$, (b1) $\beta = -1$, $\gamma_2 = -2$, (b2) $\beta = -1$, $\gamma_2 = 1$, (b3) $\beta = -1$, $\gamma_2 = 2$.

Δ_2 are both positive, and susceptible to perturbations when at least one of them is negative. The MI gain spectrum exhibits two pairs of spectral sidebands when Δ_1 and Δ_2 are both negative. Here, we define MI-A and MI-B for parameter regimes where $\Delta_1 < 0$ and $\Delta_2 < 0$, respectively. Obviously, the MI characteristics of the CW solution are determined by both MI-A and MI-B. It is also worth noting that if pairs of perturbation amplitudes are the same, i.e. $q_{11} = q_{21}$ and $q_{12} = q_{22}$ in Eq. (7), then dispersion relation (9) will reduce to a quadratic equation whose two roots are given in Eq. (11a). In that case, MI is determined solely by Δ_1 [cf. Eq. (12a)].

One may quantify MI by way of dispersion relation (9). For definiteness in the following analysis, we set $\beta = 1$ (anomalous dispersion) or $\beta = -1$ (normal dispersion). Schematic plots of the MI-A gain $G_A = 2\mathrm{Im}(K_{1,2})$ versus the frequency Ω and the coherent coupling nonlinearity γ_3 are shown in Fig. 1. It can be seen that MI-A occurs when γ_3 exceeds the threshold value $\gamma_{\mathrm{th}1} = -(\gamma_1+\gamma_2)$ for anomalous dispersion [Fig. 1(a)], but it occurs when γ_3 is less than the threshold value $\gamma_{\mathrm{th}1}$ for normal dispersion [Fig. 1(b)]. In both regimes, MI-A behaves exactly like baseband MI [Fig. 1(c)].

Fig. 2 depicts the dependence of the MI-B gain $G_B = 2\mathrm{Im}(K_{3,4})$ on Ω and γ_3 for different relations between γ_1 and γ_2. There is again a threshold value, $\gamma_{\mathrm{th}2} = \mathrm{sgn}[\beta]\cdot\max\{\mathrm{sgn}[\beta]\cdot(\gamma_1-\gamma_2), 0\}$; MI-B occurs when $\gamma_3 < \gamma_{\mathrm{th}2}$ for anomalous dispersion, and when $\gamma_3 > \gamma_{\mathrm{th}2}$ for normal dispersion. It is worth noting that there is a stable critical point $\gamma_{3c} = \gamma_2-\gamma_1$ for $\gamma_1 > \gamma_2$ in the anomalous dispersion regime, and for $\gamma_1 < \gamma_2$ in the normal dispersion regime. Fig. 3 shows cross-sectional views of the MI-B gain spectra in Fig. 2 for different γ_3. It is evident that MI-B behaves rather differently from MI-A because two other kinds of spectral structure appear in addition to the familiar baseband contribution (blue solid lines). One kind (black dash-dot lines) behaves exactly like passband MI [13,14]. The characteristics of the other (red dotted lines) are qualitatively different from those of both baseband and passband MI; this second kind is referred to as zero-baseband MI.

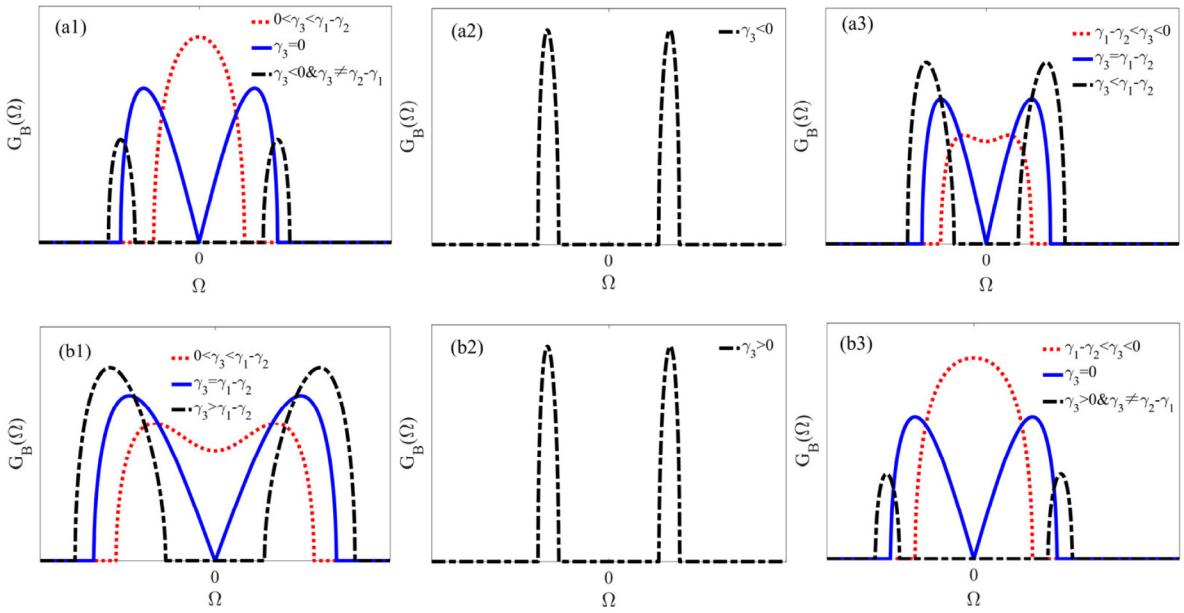

Fig. 3. The corresponding cross-sectional views of the MI-B gain spectra in Fig. 2(a1–a3) and (b1–b3) at different γ_3.

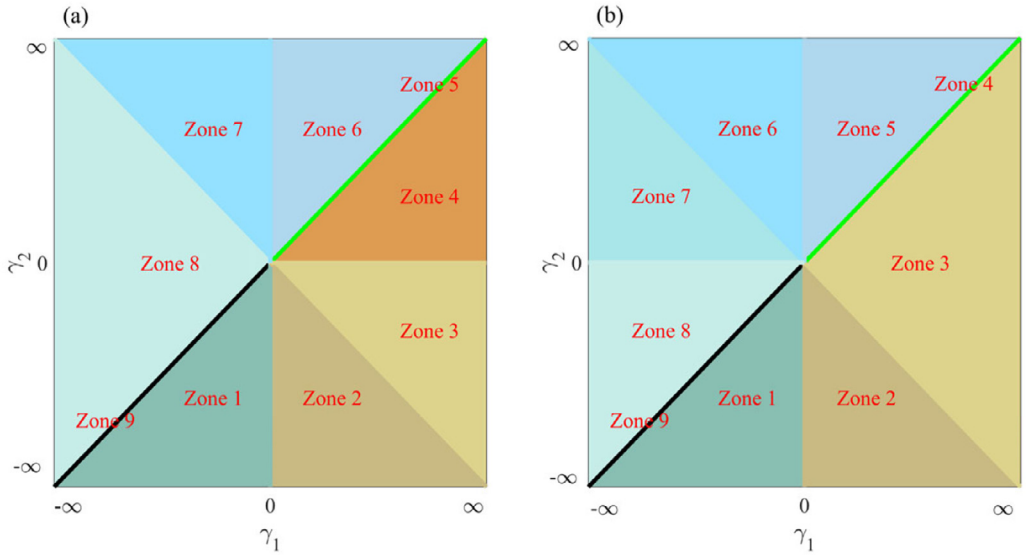

Fig. 4. Division of the $[\gamma_1 \quad \gamma_2]$ plane in the (a) anomalous and (b) normal dispersion regimes. Zones 1 to 9 for (a) and (b) are specified in the text.

As mentioned above, the instability of the CW solution is determined by both MI-A and MI-B. By comparing the values of γ_3 corresponding to the boundaries between different MI regimes in Figs. 1 and 2, the $[\gamma_1 \quad \gamma_2]$ plane in both dispersion regimes can be divided into nine zones. As shown in Fig. 4(a), the zones for anomalous dispersion are labeled Zone 1 $\gamma_2 < \gamma_1 \leq 0$, Zone 2 $0 < \gamma_1 \leq -\gamma_2$, Zone 3 $0 \leq -\gamma_2 < \gamma_1$, Zone 4 $0 < \gamma_2 < \gamma_1$, Zone 5 $\gamma_1 = \gamma_2 > 0$, Zone 6 $0 < \gamma_1 < \gamma_2$, Zone 7 $-\gamma_2 < \gamma_1 \leq 0$, Zone 8 $\gamma_1 < \gamma_2 \,\&\, \gamma_1 \leq -\gamma_2$, and Zone 9 $\gamma_1 = \gamma_2 \leq 0$. Similarly, the nine zones for normal dispersion are labeled Zone 1 $\gamma_2 < \gamma_1 \leq 0$, Zone 2 $0 < \gamma_1 \leq -\gamma_2$, Zone 3 $\gamma_1 > -\gamma_2 \,\&\, \gamma_1 > \gamma_2$, Zone 4 $\gamma_1 = \gamma_2 > 0$, Zone 5 $0 < \gamma_1 < \gamma_2$, Zone 6 $-\gamma_2 < \gamma_1 \leq 0$, Zone 7 $0 < \gamma_2 < -\gamma_1$, Zone 8 $\gamma_1 < \gamma_2 \leq 0$, and Zone 9 $\gamma_1 = \gamma_2 \leq 0$, as shown in Fig. 4(b). The dependence of MI gain on Ω and γ_3 in the different zones for anomalous and normal dispersion regions is shown in Figs. 5 and 6, respectively. It can be seen that if MI occurs, only the baseband contribution is present in both anomalous and normal regimes when the coherent coupling nonlinearity is absent ($\gamma_3 = 0$). Therefore, the existence of passband and zero-baseband contributions is due to the presence of γ_3 alone. More detailed analysis reveals that for anomalous dispersion, the introduction of $\gamma_3 < 0$ may lead to passband and zero-baseband MI, while $\gamma_3 > 0$ can lead

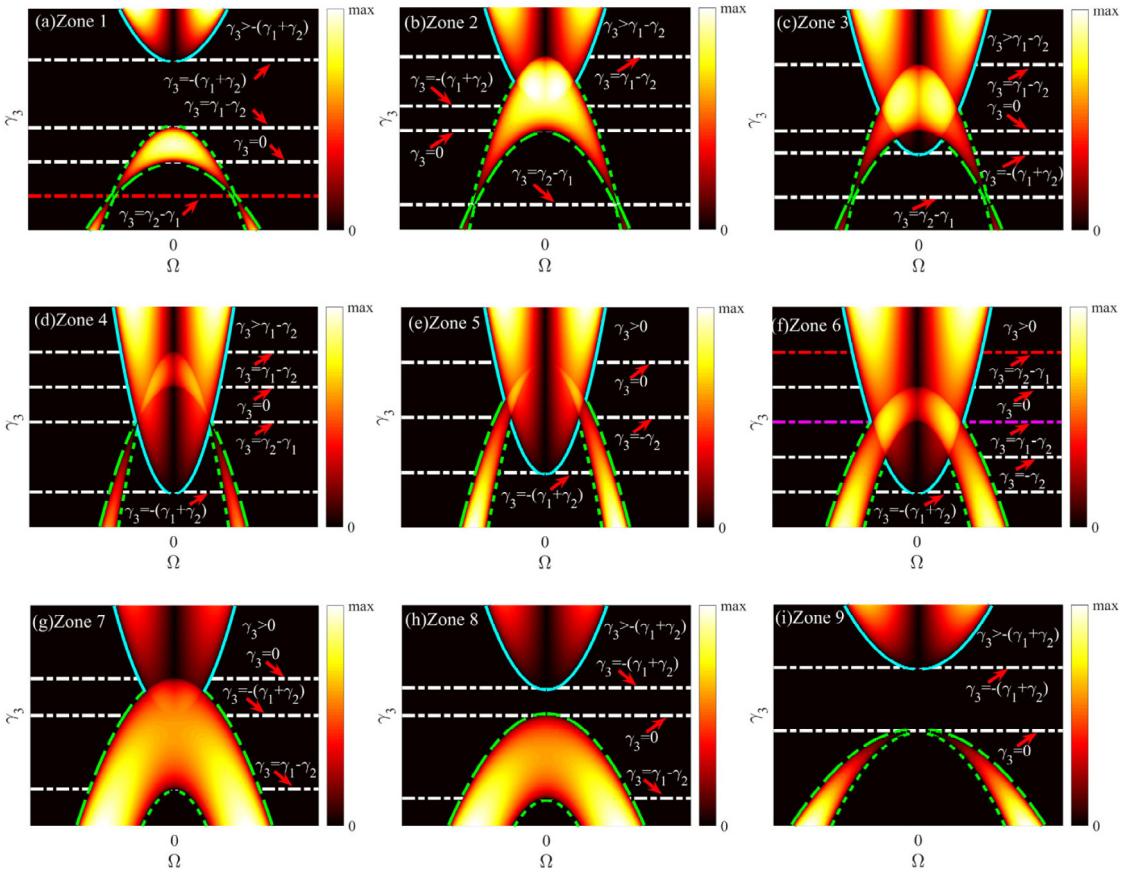

Fig. 5. Schematic plots of anomalous-dispersion MI gain as functions of frequency Ω and coherent coupling nonlinearity γ_3 for different parameter spaces located in zones 1 to 9. The adopted parameters are $\beta = 1$, (a) $\gamma_1 = -1$, $\gamma_2 = -2$, (b) $\gamma_1 = 1$, $\gamma_2 = -2$, (c) $\gamma_1 = 2$, $\gamma_2 = -1$, (d) $\gamma_1 = 2$, $\gamma_2 = 1$, (e) $\gamma_1 = 1$, $\gamma_2 = 1$, (f) $\gamma_1 = 1$, $\gamma_2 = 2$, (g) $\gamma_1 = -1$, $\gamma_2 = 2$, (h) $\gamma_1 = -2$, $\gamma_2 = 1$, (i) $\gamma_1 = -1$, $\gamma_2 = -1$.

only to zero-baseband MI (see Fig. 5). However, for normal dispersion, the introduction of $\gamma_3 < 0$ can lead only to zero-baseband MI, while $\gamma_3 > 0$ may lead to passband and zero-baseband MI (see Fig. 6). It should be noted that the above results are based on the analysis of CW solution (2).

3. RW excitation by localized perturbation in different parameter spaces

Having been fairly exhaustive exploring MI in Section 2, it is clear that there are many new possible avenues for potential RW excitation. Using the split-step Fourier method, we now perform simulations in different parameters spaces to solve perturbed initial-value problems of the form

$$u(0,t) = u_{01}(0,t)[1 + g_1(t)], \tag{13a}$$

$$v(0,t) = v_{01}(0,t)[1 + g_2(t)], \tag{13b}$$

where $g_i(t)$ $(i = 1, 2)$ denotes local disturbances at $z = 0$. Three common forms for perturbations were tested: Gaussian $g_i(t) = \varepsilon_i \exp[-(t - t_{0i})^2/w_i]$, super-Gaussian $g_i(t) = \varepsilon_i \exp[-(t - t_{0i})^4/w_i]$, and hyperbolic secant $g_i(t) = \varepsilon_i \mathrm{sech}[(t - t_{0i})/w_i]$ [36,37], where in each case the real constants ε_i, w_i, and t_{0i} determine the initial amplitudes, widths, and positions, respectively. The simulations were found to be largely independent of whatever form was used, which is a finding consistent with Ref. [36]. Hence, for illustrative purposes, only a selection of results for Gaussian perturbations is shown here.

We begin by considering the evolution of an in-phase wave when the two initial perturbations differ from one another, i.e. $g_1(t) \neq g_2(t)$. Fig. 7(a)–(d) present typical numerical solutions from the various parameter spaces in Fig. 5(a), where baseband MI, modulation stability, zero-baseband MI and passband MI occur, respectively. These simulations show that a RW (highlighted by a red dashed ellipse) can be excited in the parameter spaces for baseband and zero-baseband MI [Fig. 7(a) and (c)]. However, the solution splits into sets of pulses in the parameter spaces for modulation stability and

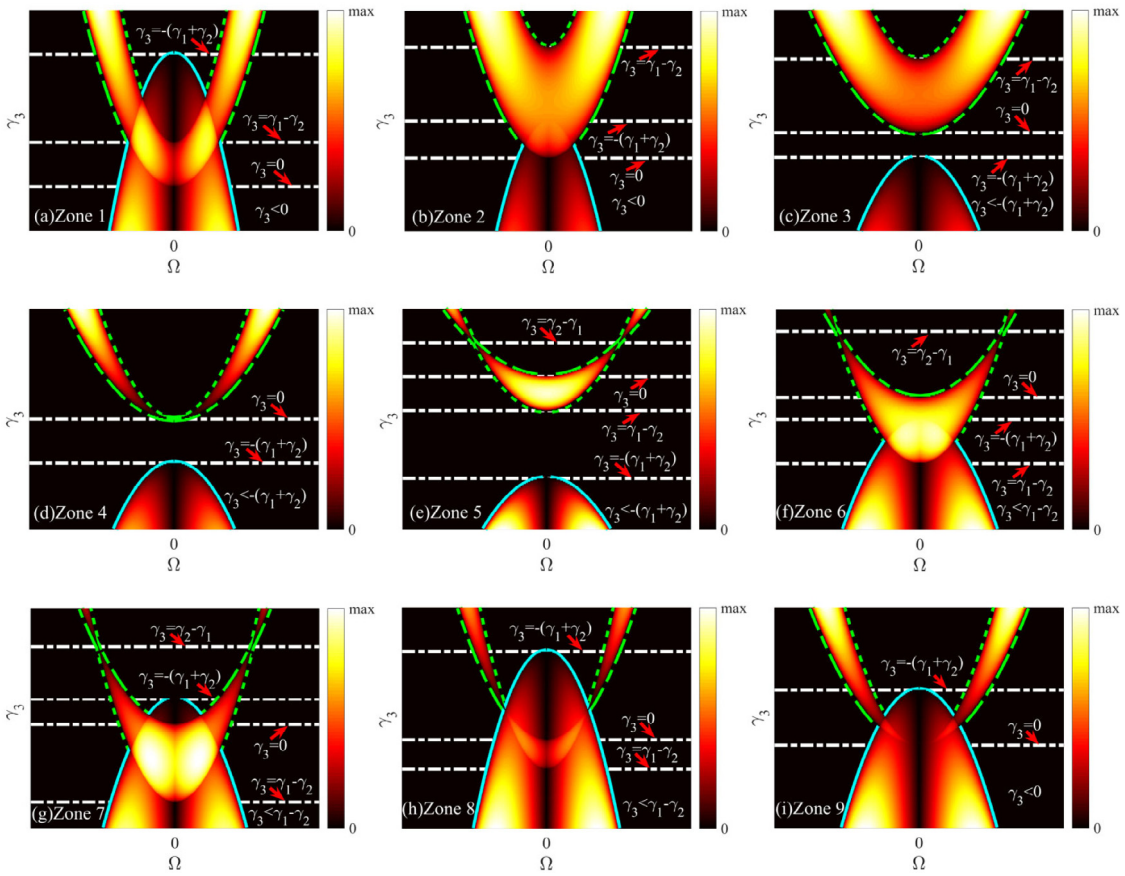

Fig. 6. Schematic plots of the normal-dispersion MI gain as functions of frequency Ω and coherent coupling nonlinearity γ_3 for different parameter spaces located in zones 1 to 9. The adopted parameters are $\beta = -1$, (a), $\gamma_1 = -1$, $\gamma_2 = -2$, (b) $\gamma_1 = 1$, $\gamma_2 = -2$, (c) $\gamma_1 = 2$, $\gamma_2 = -1$, (d) $\gamma_1 = 1$, $\gamma_2 = 1$, (e) $\gamma_1 = 1$, $\gamma_2 = 2$, (f) $\gamma_1 = -1$, $\gamma_2 = 2$, (g) $\gamma_1 = -2$, $\gamma_2 = 1$, (h) $\gamma_1 = -2$, $\gamma_2 = -1$, (i) $\gamma_1 = -1$, $\gamma_2 = -1$.

passband MI [Fig. 7(b) and (d)]. Moreover, the maximal intensity of the RW in the case of zero-baseband MI is somewhat smaller than that in the case of baseband MI [compare Fig. 7(c) and (a)].

We have also performed extensive simulations of the in-phase CW solution in different parameter spaces of Figs. 5(b-i) and 6, along with the corresponding out-of-phase CW solution. The results were always consistent with those presented in Fig. 7 though, for brevity, they are omitted here. The key physical prediction to emerge is that a RW can be excited from both in-phase and out-of-phase CW solutions in parameter spaces where baseband or zero-baseband MI occur. In contrast, perturbations to an in-phase or out-of-phase CW solution tend to cause a splitting into pulses in parameter spaces where passband MI or modulation stability occurs.

Combining the analysis of MI with supporting simulations, it can be inferred that when MI occurs, a RW can be excited if $\gamma_3 > \gamma_{\text{th3}} = \min[0, \gamma_1 - \gamma_2, -(\gamma_1 + \gamma_2)]$ in the anomalous dispersion regime, or if $\gamma_3 < \gamma_{\text{th4}} = \max[0, \gamma_1 - \gamma_2, -(\gamma_1 + \gamma_2)]$ in the normal dispersion regime. Some special cases of these results have been reported elsewhere. Based on system (1) with $\beta = 1/2$, $\gamma_1 = \gamma_3 = \sigma$ and $\gamma_2 = 2\sigma$, Ling et al. [38] obtained the RW solution for $\sigma = 1$ but reported soliton solutions only for $\sigma = -1$; Zhang et al. [39] found that MI occurs when $\sigma = 1$ and that modulation stability appears for $\sigma = -1$. In our work, the parameter space with $\sigma = 1$ corresponds to the red line in Fig. 5(f), where baseband MI appears; the parameter space with $\sigma = -1$ corresponds to the stable critical point shown by red line in Fig. 5(a). Sun et al. [40] took the in-phase CW solutions as a seed and obtained RWs via the Darboux transformation of system (1) with $\beta = 1$, $\gamma_1 = 2$, $\gamma_2 = 4$, and $\gamma_3 = -2$. The parameter space in Ref. [40] corresponds to the magenta line in Fig. 5(f), where baseband MI occurs. Obviously, the conclusions presented here are more general.

Finally, we consider the evolution of CW solutions subject to identical initial perturbations, i.e. $g_1(t) = g_2(t)$. As mentioned in Section 2, when the perturbations in the two components are the same, dispersion relation (9) possesses only one pair of roots $K_{1,2}$, so that MI is completely determined by MI-A. In such a scenario, only baseband MI exists. Fig. 8(a)–(d), respectively, show a set of simulations for perturbed in-phase CW solutions under the condition $g_1(t) = g_2(t)$ for the different parameter spaces of Fig. 5(a). It can be seen that a RW (highlighted by the red dashed ellipse) can be excited from a perturbed in-phase CW solution in the parameter space where baseband MI occurs, while the same solution splits into smaller pulses in other parameter spaces (which is agreement with the analysis in Section 2).

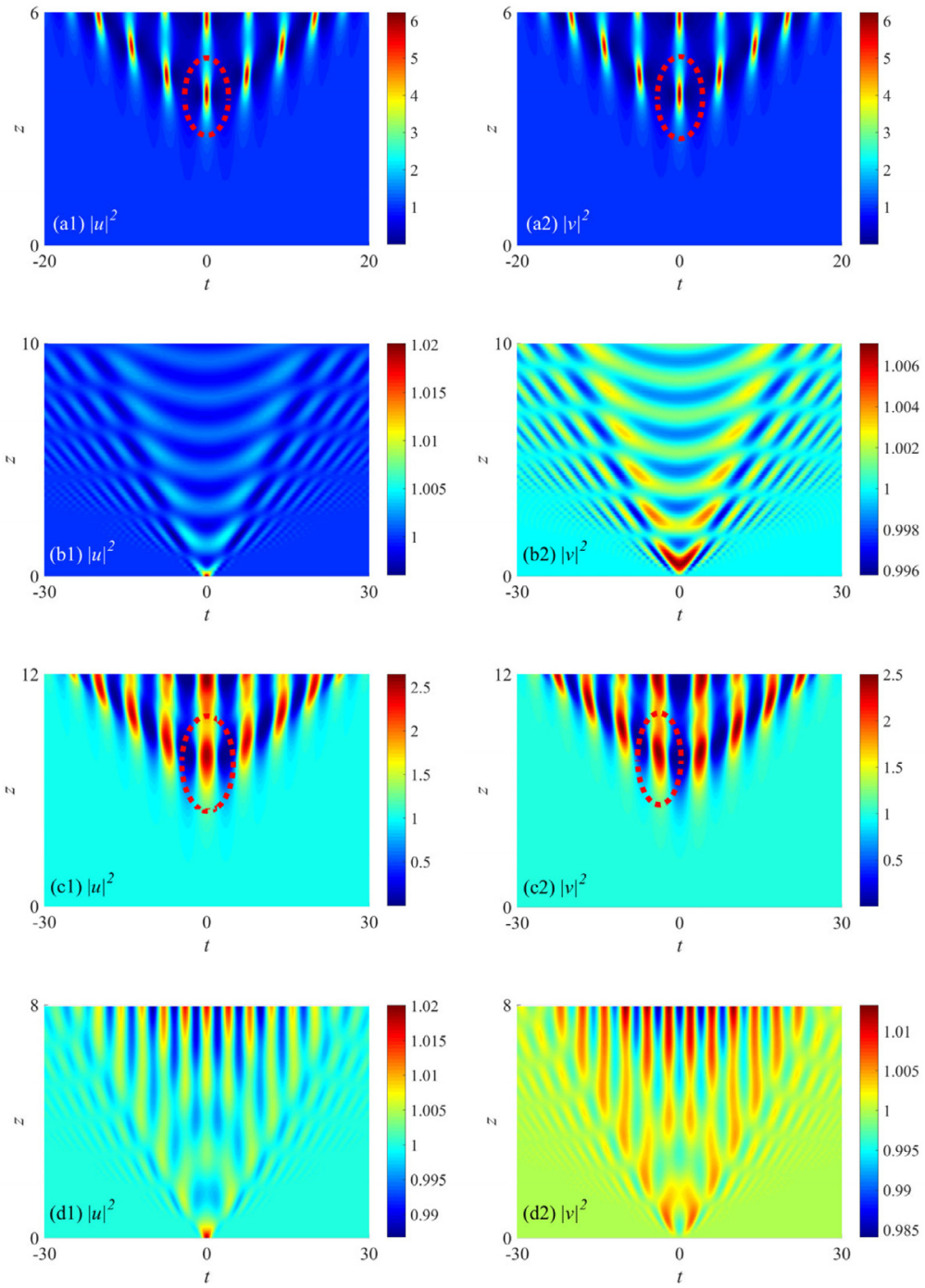

Fig. 7. Typical numerical results for the in-phase CW solution with Gaussian perturbations for different parameter spaces in Fig. 5(a) when $g_1(t) \neq g_2(t)$. γ_1, γ_2, and γ_3 are located in the parameter spaces of Fig. 5(a), where (a) baseband MI, (b) modulation stability, (c) zero-baseband, and (d) passband MI occur. The other parameters are $\varepsilon_1 = 0.01$, $w_1 = 0.5$, $t_{01} = 0$, $\varepsilon_2 = 0$. A RW is highlighted by a red dashed ellipse in (a) and (c).

4. Conclusions

In the framework of coherently coupled system (1), we have mapped out the MI characteristics of the in-phase and out-of-phase CW solutions in both anomalous and normal dispersion regimes. It has been found that when the initial perturbations in the two components are identical, only baseband MI can occur. However, when the initial perturbations

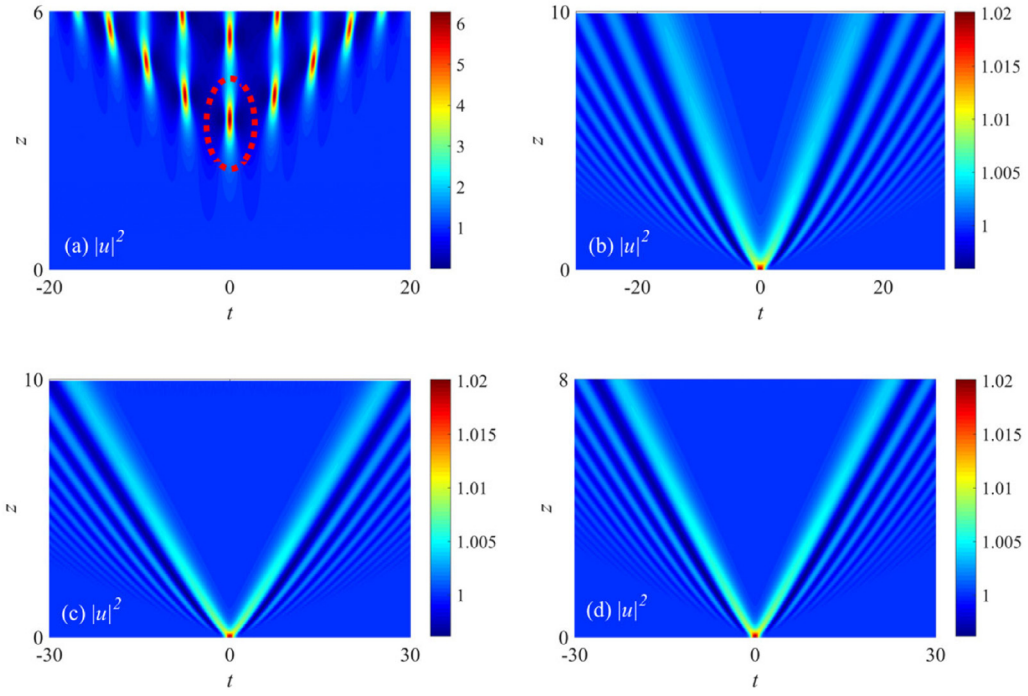

Fig. 8. Typical numerical results for the in-phase CW solution with Gaussian perturbations for different parameter spaces in Fig. 5(a) when $g_1(t) = g_2(t)$. The adopted parameters in (a–d) are the same as those in Fig. 7(a–d), respectively, except for $\varepsilon_2 = 0.01$, $w_2 = 0.5$, and $t_{02} = 0$. A RW is highlighted by a red dashed ellipse in (a), and only the u component is presented (the v component shows very similar behavior).

are different (thereby introducing a symmetry-breaking element), there appears a richer and much more intricate spectral structure: baseband, passband, and zero-baseband MI. Moreover, one may attribute coherent coupling nonlinearity directly to the existence of passband and zero-baseband MI phenomena.

Based on the analysis of dispersion relation (9), we have addressed numerically the possibility of exciting RWs from in-phase and out-of-phase CW solutions (subject to Gaussian perturbations) in those parameter spaces where three types of MI are supported. Simulations have revealed that RWs emerge only when baseband or zero-baseband MI occur. Moreover, the peak intensities of RWs in the zero-baseband case are typically less than those in the baseband case.

By combining analysis and numerics, we have found that when MI is present, RWs can be generated by perturbing either in-phase or out-of-phase CW solutions if γ_3 exceeds the threshold γ_{th3} in the anomalous dispersion regime, or if γ_3 falls below the threshold γ_{th4} in normal dispersion regime. Our results, thus, extend over the entire parameter space of system (1) and, in that way, go beyond what has been published to date [27,39]. Moreover, the thresholds reported here are key research findings that are essential for identifying regions of parameter space capable of supporting RW formation without needing to solve system (1) directly.

CRediT authorship contribution statement

Heping Jia: Writing – original draft, Numerical simulations, Data analysis. **Rongcao Yang:** Conceptualization, Validation. **Qi Guo:** Conceptualization. **J.M. Christian:** Writing – review & editing.

Declaration of competing interest

The authors declare that they have no known competing financial interests or personal relationships that could have appeared to influence the work reported in this paper.

Acknowledgments

This work was supported by National Natural Science Foundation of China [grant number 61775126]; and the Natural Science Foundation of Shanxi Province [grant number 201801D221164]

References

[1] Peregrine DH. Water waves, nonlinear Schrödinger equations and their solutions. J Aust Math Soc B 1983;25:16.
[2] Solli DR, Ropers C, Koonath P, Jalali B. Optical rogue waves. Nature 2007;450:1054.
[3] Bludov YV, Konotop VV, Akhmediev N. Matter rogue waves. Phys Rev A 2009;80:033610.
[4] Chabchoub A, Hoffmann NP, Akhmediev N. Rogue wave observation in a water wave tank. Phys Rev Lett 2011;106:204502.
[5] Chen S, Baronio F, Soto-Crespo JM, Grelu P, Mihalache D. Versatile rogue waves in scalar, vector, and multidimensional nonlinear systems. J Phys A 2017;50:463001.
[6] Akhmediev N. Waves that appear from nowhere: complex rogue wave structures and their elementary particles. Front Phys 2021;8:612318.
[7] Mihalache D. Localized structures in optical and matter-wave media: a selection of recent studies. Rom Rep Phys 2021;73:403.
[8] Onorato M, Residori S, Bortolozzo U, Montina A, Arecchi FT. Rogue waves and their generating mechanisms in different physical contexts. Phys Rep 2013;528:47.
[9] Akhmediev N, Soto-Crespo JM, Ankiewicz A. Extreme waves that appear from nowhere: On the nature of rogue waves. Phys Lett A 2009;373:2137.
[10] Kharif C, Pelinovsky E. Physical mechanisms of the rogue wave phenomenon. Eur J Mech B Fluids 2003;22:603.
[11] Pan C, Bu L, Chen S, Mihalache D, Grelu P, Baronio F. Omnipresent coexistence of rogue waves in a nonlinear two-wave interference system and its explanation by modulation instability. Phys Rev Res 2021;3:033152.
[12] Chen JB, Pelinovsky DE, White RE. Periodic standing waves in the focusing nonlinear Schrödinger equation: Rogue waves and modulation instability. Physica D 2020;405:132378.
[13] Baronio F, Conforti M, Degasperis A, Lombardo S, Onorato M, Wabnitz S. Vector rogue waves and baseband modulation instability in the defocusing regime. Phys Rev Lett 2014;113:034101.
[14] Baronio F, Chen S, Grelu P, Wabnitz S, Conforti M. Baseband modulation instability as the origin of rogue waves. Phys Rev A 2015;91:0330804.
[15] Zhao LC, Ling L. Quantitative relations between modulational instability and several well-known nonlinear excitations. J Opt Soc Amer B 2016;33:850.
[16] Chen JB, Pelinovsky DE, Upsal J. Modulational instability of periodic standing waves in the derivative NLS equation. J Nonlinear Sci 2021;31:58.
[17] Chen JB, Pelinovsky DE. Rogue waves on the background of periodic standing waves in the derivative nonlinear Schrödinger equation. Phys Rev E 2021;103:062206.
[18] Dudley JM, Genty G, Coen S. Supercontinuum generation in photonic crystal fiber. Rev Modern Phys 2006;78:1135.
[19] Hasegawa A. Generation of a train of soliton pulses by induced modulational instability in optical fibers. Opt Lett 1984;9:288.
[20] Agrawal GP. Nonlinear fiber optics. New York: Academic; 2007, p. 120–9.
[21] Vanderhaegen G, Naveau C, Szriftgiser P, Kudlinski A, Conforti M, Mussot A, Onorato M, Trillo S, Chabchoub A, Akhmediev N. Extraordinary modulation instability in optics and hydrodynamics. Proc Natl Acad Sci USA 2021;118:e2019348118.
[22] Agrawal GP. Modulation instability induced by cross-phase modulation. Phys Rev Lett 1987;59:880.
[23] Berkhoer AL, Zakharov VE. Self excitation of waves with different polarizations in nonlinear media. Zh Eksp Teor Fiz 1970;58:903; Sov Phys J Exp Theor Phys 1970;31:486.
[24] Rothenberg JE. Modulational instability for normal dispersion. Phys Rev A 1990;42:682.
[25] Drummond PD, Kennedy TAB, Dudley JM, Leonhardt R, Harvey JD. Cross-phase modulational instability in high-birefringence fibers. Opt Commun 1990;78:137.
[26] Chan HN, Malomed BA, Chow KW, Ding E. Rogue waves for a system of coupled derivative nonlinear Schrödinger equations. Phys Rev E 2016;93:012217.
[27] Chiu HS, Chow KW. Effect of birefringence on the modulation instabilities of a system of coherently coupled nonlinear Schrödinger equations. Phys Rev A 2009;79:065803.
[28] Ye YL, Liu J, Bu LL, Pan CC, Chen SH, Mihalache D. Rogue waves and modulation instability in an extended Manakov system. Nonlinear Dyn 2020;102:1801–12.
[29] Sun WR, Liu L. Asymmetrical, rotational and ultra-high amplitude fundamental polarized optical rogue waves associated with the coherent coupling. Phys Lett A 2021;391:127132.
[30] Jia HP, Li B, Yang RC, Tian JP. Diverse composite waves in coherently coupled inhomogeneous fiber systems with external potentials. Nonlinear Dynam 2020;99:2987.
[31] Hu X, Guo J, Zhao LM, Ma J, Tang DY. Coherently coupled vector black solitons in a quasi-isotropic cavity fiber laser. Opt Lett 2020;45:6563.
[32] Mareeswaran RB, Kanna T. Superposed nonlinear waves in coherently coupled Bose–Einstein condensates. Phys Lett A 2016;380:3244.
[33] Manakov SV. On the theory of two-dimensional stationary self-focusing of electromagnetic waves. Zh Eksp Teor Fiz 1973;65:505, English translation:; Sov Phys JETP 1974;38:248.
[34] Yue YF, Huang LL, Chen Y. Modulation instability, rogue waves and spectral analysis for the sixth-order nonlinear Schrödinger equation. Commun Nonlinear Sci Numer Simul 2020;89:105284.
[35] Xiang YJ, Wen SC, Dai XY, Fan DY. Modulation instability in nonlinear oppositely directed coupler with a negative-index metamaterial channel. Phys Rev E 2010;82:056605.
[36] Gao P, Zhao LC, Yang ZY, Li XH, Yang WL. High-order rogue waves excited from multi-Gaussian perturbations on a continuous wave. Opt Lett 2020;45:2399.
[37] Wang QY, Liu DM, Li XH. Transformation point on the peak intensity of high-order rogue wave and its critical behavior. Commun Nonlinear Sci 2019;75:302.
[38] Ling LM, Zhao LC. Integrable pair-transition-coupled nonlinear Schrödinger equations. Phys Rev E 2015;92:022924.
[39] Zhang GQ, Yan ZY, Wen XY. Modulational instability, beak-shaped rogue waves, multi-dark-dark solitons and dynamics in pair-transition-coupled nonlinear Schrödinger equations. Proc Math Phys Eng Sci 2017;473:20170243.
[40] Sun WR, Tian B, Jiang Y, Zhen HL. Optical rogue waves associated with the negative coherent coupling in an isotropic medium. Phys Rev E 2015;91:023205.